**SIRM 2015 – 11th International Conference on Vibrations in Rotating Machines,
Magdeburg, Deutschland, 23. – 25. February 2015**

Reliability analysis of mistuned blisks

Nils Wagner [1], **Reinhard Helfrich** [2]

[1] Intes GmbH, Schulze-Delitzsch-Str. 16, D-70565, Stuttgart, Germany, nils.wagner@intes.de
[2] Intes GmbH, Schulze-Delitzsch-Str. 16, D-70565, Stuttgart, Germany, reinhard.helfrich@intes.de

Abstract

Blisks also known as bladed disks are designed to be cyclic structures. However, tolerances in the manufacturing and assembling processes and wear originate a loss of symmetry. This phenomenon is called mistuning effect. These imperfections inherently influence the dynamic behaviour of the rotor. It turns out that they can drastically influence the forced response levels. These imperfections could cause large increases in stress and vibration amplitudes. Hence the demand for computationally effective methods to predict and quantify such systems is of great interest to the manufacturers of turbine engines. Due to the spatial confinement of vibration energy, certain blades in a mistuned system can suffer damage by significant forced-response vibration amplitudes compared to the ideal (tuned) system.In the absence of mistuning the dynamics of blisks is fully determined from that of a small portion, typically a bladed sector. For this reason mistuning was investigated by lumped models in the past. Nowadays full scale finite element models are available. They take advantage of modelling the shape and flexibility of the blades in a realistic manner. The mistuning effect is often idealized by a modification of mass and stiffness distribution inside the blades. This can be achieved by random mass and stiffness variations or fuzzy variables. In this study the effect of stiffness mistuning on the forced response of a rotating blisk excited by different engine orders is investigated. Uncertainties in rotors arise for example from in-use wear of the blades, temperatur fluctuations and from manufacturing tolerances.

1 Introduction

The effects of mistuning on the free and forced response of blisks is of great interest. The theoretical background of tuned disks is related to circulant matrices [20]. In the early days lumped-parameter models [18, 26, 27, 30, 32] have been used to investigate various kinds of mistuning. However most of these studies neglected the effects due to rotation. Nowadays quite complex threedimensional models are available [1, 13, 22, 25]. They take advantage of modelling the shape and flexibility of the blades in a realistic manner. The mistuning effect is often idealized by a modification of mass and stiffness distribution inside the blades. A simplifying assumption is often used when modeling mistuning, namely, that mistuning is proportional [15]. That means that the physical variations in each sector are considered to be proportional to the mass and/or stiffness matrices of the tuned sector. Mistuning is introdced in several ways e.g. by random mass and stiffness variations [26, 28] or fuzzy variables [8]. A blade to blade variation of damping is analyzed in [9]. Geometric mistuning is discussed in [2, 5, 31]. Aerodynamic effects as well as friction dampers are neglected here and can be found elsewhere [23, 24]. Even more sophisticated multistage disk models can be handled [10, 11, 33].

The blisk geometry is taken from [16] and has been modeled and analyzed using the PERMAS finite element program [34]. The disk has 20 blades evenly spaced around the cicumference. The Youngs modulus of even and odd blade numbers will be chosen as random parameters, respectively. Beside the geometric and centrifugal stiffness matrix, the Coriolis matrix is taken into account [19]. Different engine order excitations are considered in a forced response, whereas unbalance loads are usually neglected.

2 Equations of motion

The governing equations of motion that describes a rotor system in a co-rotating reference frame is given by

$$\boldsymbol{M}\,\ddot{\boldsymbol{u}} + (\boldsymbol{D} + \boldsymbol{D}_c)\,\dot{\boldsymbol{u}} + (\boldsymbol{K} + \boldsymbol{K}_g + \boldsymbol{K}_z)\,\boldsymbol{u} = \boldsymbol{R}(t), \tag{1}$$

where $\boldsymbol{M}$ denotes the mass matrix, $\boldsymbol{D}$ viscous damping matrix. $\boldsymbol{D}_c$ Coriolis matrix. $\boldsymbol{K}_z$ centrifugal stiffness matrix, $\boldsymbol{K}_g$ geometric stiffness matrix, $\boldsymbol{K}$ structural stiffness matrix and $\boldsymbol{R}(t)$ external forces. The first computation step is a static analysis for the basic model to determine the stress distribution under centrifugal loads. It is a prerequisite for the calculation of the geometric stiffness matrix $\boldsymbol{K}_g$. The next step is the calculation of real eigenmodes $\boldsymbol{Y} = \begin{bmatrix} \boldsymbol{y}_1 \ \dots \ \boldsymbol{y}_r \end{bmatrix}$, including geometric and centrifugal stiffness matrices

$$\boldsymbol{M}\,\boldsymbol{Y} = (\boldsymbol{K} + \boldsymbol{K}_g + \boldsymbol{K}_z)\,\boldsymbol{Y}\,\boldsymbol{\Lambda}, \quad \boldsymbol{\Lambda} = \begin{bmatrix} \lambda_1 & & \\ & \ddots & \\ & & \lambda_r \end{bmatrix}, \quad \lambda_i = \frac{1}{\omega_i^2}, \quad \boldsymbol{M} \in \mathbb{R}^{n \times n}. \tag{2}$$

The number of eigenfrequencies and modeshapes is equal to the number of degrees of freedom n of the system. However, engineering experiences indicate that only the first few eigenmodes are required to obtain the response with sufficient accuracy, i.e. ($r \ll n$). For a perfectly tuned system, the number of repeated eigenvalue sets equals $(n-1)/2$ and $(n-2)/2$ for odd and even number of blades n [32]. Additional matrices due to rotation are requested by a so-called $ADDMATRIX block in PERMAS, i.e.

```
$ADDMATRIX
  GEOSTIFF CENTRISTIFF CORIOLIS
```

The equations of motion (1) are transformed into modal space

$$\widetilde{\boldsymbol{M}}\,\ddot{\boldsymbol{\eta}} + \left(\widetilde{\boldsymbol{D}} + \widetilde{\boldsymbol{D}}_c\right)\,\dot{\boldsymbol{\eta}} + \left(\widetilde{\boldsymbol{K}} + \widetilde{\boldsymbol{K}}_g + \widetilde{\boldsymbol{K}}_z\right)\,\boldsymbol{\eta} = \widetilde{R}(t) \tag{3}$$

by means of $\boldsymbol{u} = \boldsymbol{Y}\,\boldsymbol{\eta}$. The complex eigenvalue problem

$$\lambda \begin{bmatrix} -\widetilde{\boldsymbol{M}} & \boldsymbol{O} \\ \boldsymbol{O} & \boldsymbol{I}_r \end{bmatrix} \boldsymbol{z} = \begin{bmatrix} \widetilde{\boldsymbol{D}} + \widetilde{\boldsymbol{D}}_c & \widetilde{\boldsymbol{K}} + \widetilde{\boldsymbol{K}}_g + \widetilde{\boldsymbol{K}}_z \\ \boldsymbol{I}_r & \boldsymbol{O} \end{bmatrix} \boldsymbol{z}, \quad \boldsymbol{z} = \begin{bmatrix} \lambda\boldsymbol{\eta} \\ \boldsymbol{\eta} \end{bmatrix} \tag{4}$$

is repeatedly solved in modal state-space for various rotational speeds of the blisk to achieve the relation between eigenfrequencies and rotational speed. A mode tracking algorithm is implemented in order to sort the complex eigenvalues.

3 Reliability analysis

The stochastic analysis of a design assumes some properties of a structure or the loads to be uncertain, knowing only the characteristics of their probability distributions. The procedure in a reliability analysis comprises the following steps.

Definition of uncertain quantities like physical, geometrical or loads in structural analysis by basic variables.
Definition of limit state (or failure) functions related to quantities of a structural analysis.
Calculation of the probability of failure for each limit state function.

Several reliablity methods are available in PERMAS. FORM and SORM are not applicable here due to missing derivatives. Therefore we focus on adaptive Monte Carlo simulations. In the context of mistuned blisks Monte Carlo simulations are used in [12]. A large number of simulations will provide an appropriate estimate for the probability of failure. Rough estimates of failure probabilities can be obtained with

$$m = 10(P_F)^{-1}. \tag{5}$$

Therefore, investigations of failure probabilities in the regime of 10^{-5} to 10^{-8} may require a million to a billion trials for even rough estimates [7]. However, time and the power of computers are limited. In order to achieve an acceptable level of accuracy an upper bound of the coefficient of variation for the probability of failure can be defined. Alternative computational options are crude Monte Carlo and RSM [4].

Table 1: Geometrical and physical properties of the blisk

	Blades	Disk
Spanwise length [m]	$2.159\,10^{-1}$	–
Chordwide width [m]	$1.651\,10^{-1}$	–
Thickness [m]	$1.524\,10^{-2}$	$1.651\,10^{-1}$
Outer diameter [m]	-	$5.1816\,10^{-1}$
Inner diameter [m]	-	$7.62\,10^{-2}$
Stagger angle [$^\circ$]	60	-
Poisson ratio	0.3	0.3
Youngs modulus [Pa]	X_1, X_2	$1.1024\,10^{11}$
Density [kg m^{-3}]	$4.5\,10^3$	$4.5\,10^3$
Modal damping	0.01	0.01
Rotor speed [rpm]	10700	10700

4 Example

The topology of the example is taken from [17]. The blisk consists of $N = 20$ blades. Each blade is discretized by 5808 linear hexaeder elements, whereas the hollow disc is idealized through 50688 hexaeder elements. LOADA elements on the surface of the model might be used to extract element stresses on the hull. The coupling of the blades and discs is achieved by a multipoint constraint ($MPC ISURFACE) definition. Displacements at the inner bore diameter are suppressed, i.e. $u = v = w = 0$. The finite element model consists of a total of $n = 610416$ degrees of freedom.

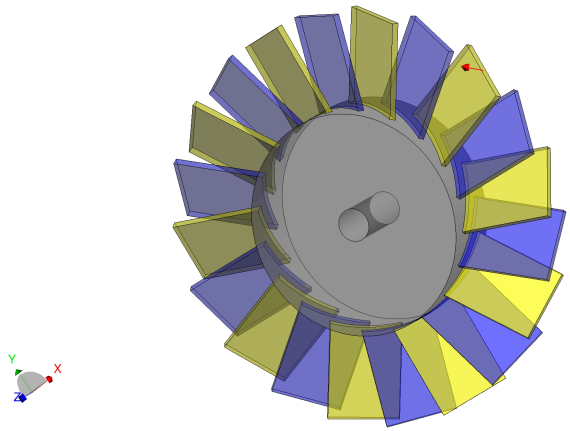

Figure 1: Idealized 20-bladed disk

4.1 Free vibration

The real eigenfrequencies of the tuned system are depicted in Fig (2). Spectral gaps are inherently present in case of a tuned blisk. Certain mode shapes can be identified from an associated strain energy distribution plot Fig. (3). Each column represents an eigenfrequency of the rotating system. It becomes apparent that the first mode (first column) in Fig. (3) is characterised by a uniform contribution of all blades. The associated mode is shown in Fig. (6(a)). A nodal diameter plot is given in Fig. (5). It turns out that the eigencurves in the Campbell diagram are subjected to a *modal spreading* effect [16] in case of a mistuned blisk Fig.(7(b)).

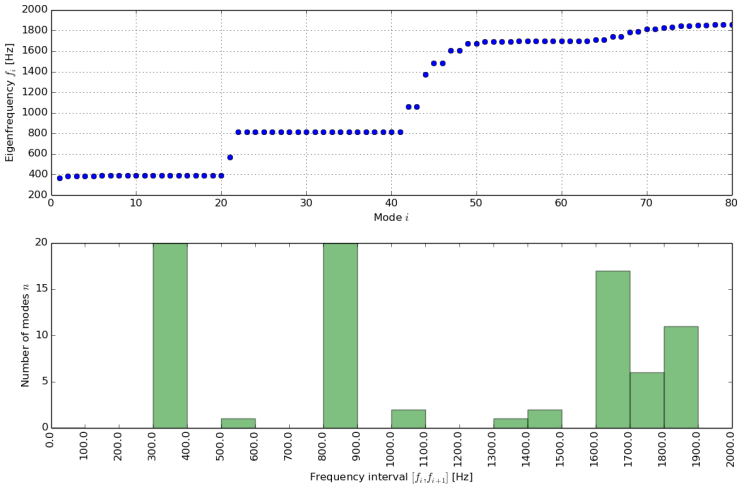

Figure 2: Cyclic frequencies of the tuned blisk ($\Omega = 10700$ rpm

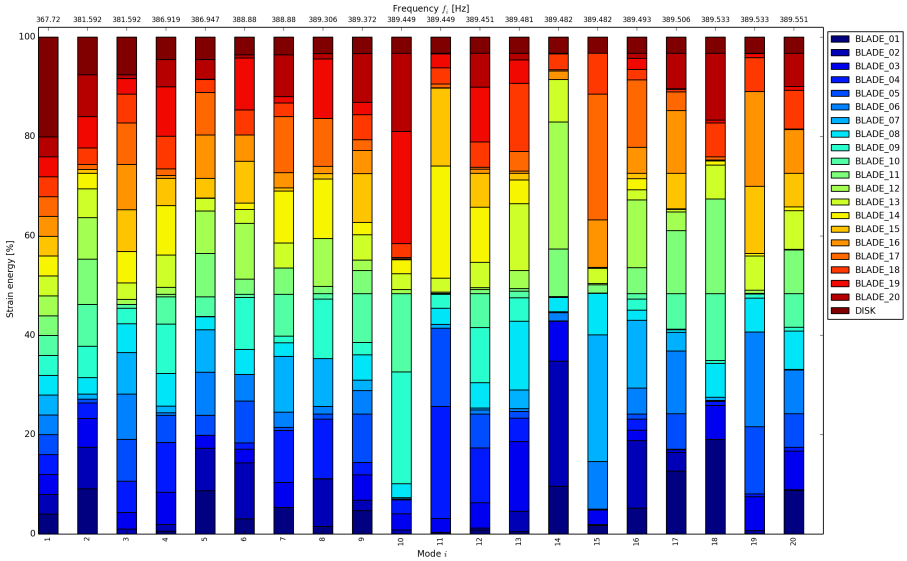

Figure 3: Strain energy distribution of the tuned disk for mode shapes 1-20 ($\Omega = 10700$ rpm)

4.2 Forced response

A unit force (characterized by a red arrow in Fig. (1)) normal to each blade surface was applied to one of the nodes at the tip of each blade. Engine order excitation is the effective travelling wave excitation that a blisk experiences as it rotates through the unsteady flow [14]. Thus the forcing function was assumed to be harmonic in time and differs only in phase from blade to blade. The phase at the $i-$th blade is given by

$$\Theta_i = \frac{2\,\pi\,C\,(i-1)}{N}, \tag{6}$$

where C is the (integer) engine order of excitation and

$$\Theta = 2\,\pi\,\frac{C}{N} \tag{7}$$

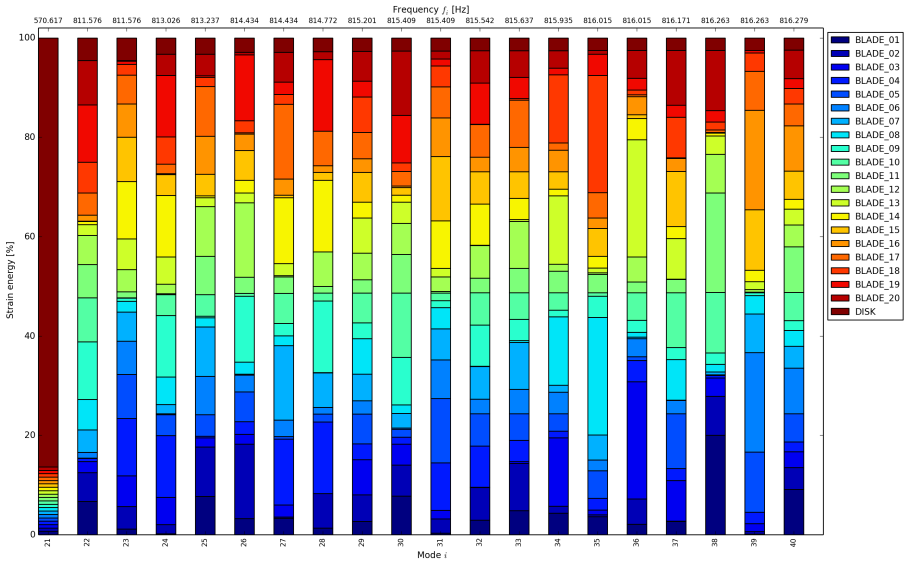

Figure 4: Strain energy distribution of the tuned disk for mode shapes 21-40 ($\Omega = 10700$ rpm)

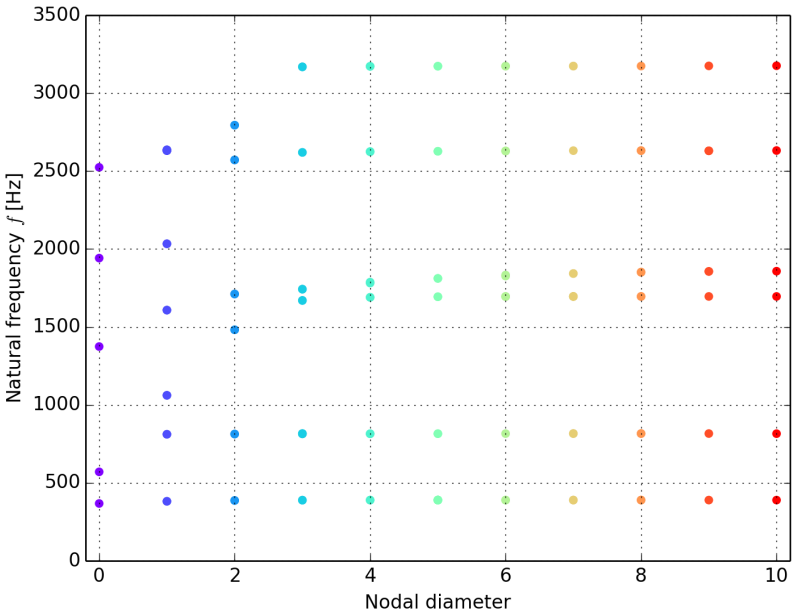

Figure 5: Nodal diameter map of the rotating idealized 20-bladed disk($\Omega = 10700$ rpm)

denotes the interblade phase angle. The forced response of a fully mistuned blisk including 20 basis variables is depicted in Fig (8(a)). The resonant peaks of the different blades are very widespread as opposed to the tuned blisk. Moreover, there is a remarkable response amplification of the mistuned bladed disk as opposed to the tuned blisk [29]. Thus the variable of interest is the maximum blade response.

4.3 Mistuning

Mistuning is introduced by changes in Young's moduli of blades. In order to reduce the number of basic variables we assume that there are only two distinct nominal blades, type A and type B, arranged in the alternating pattern $ABAB \ldots AB$ as depicted in Fig. 1. The statistical parameters of the basic variables are listed in Table 2.

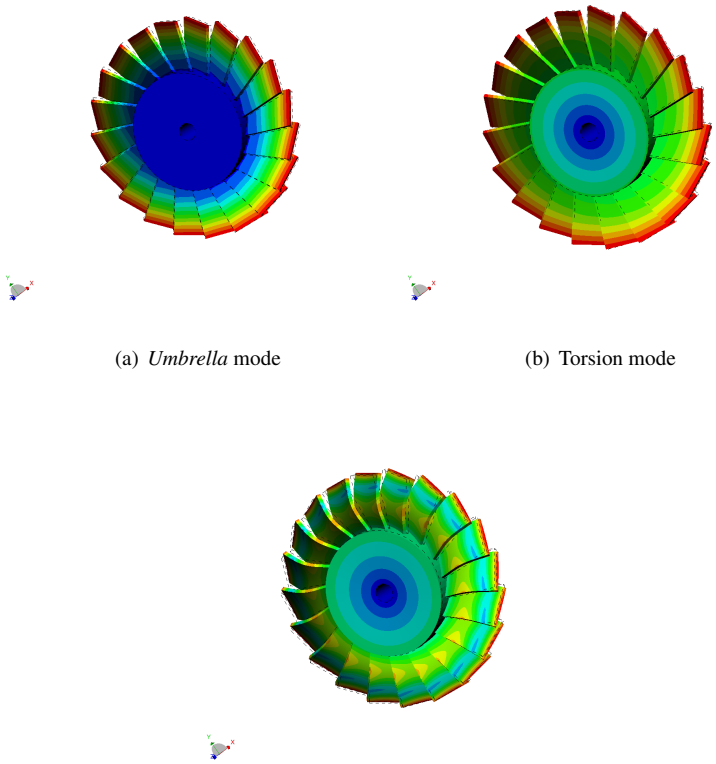

(a) *Umbrella* mode (b) Torsion mode

(c) Blisk bending mode

Figure 6: Different mode shapes of the tuned disk ($\Omega = 10700$ rpm)

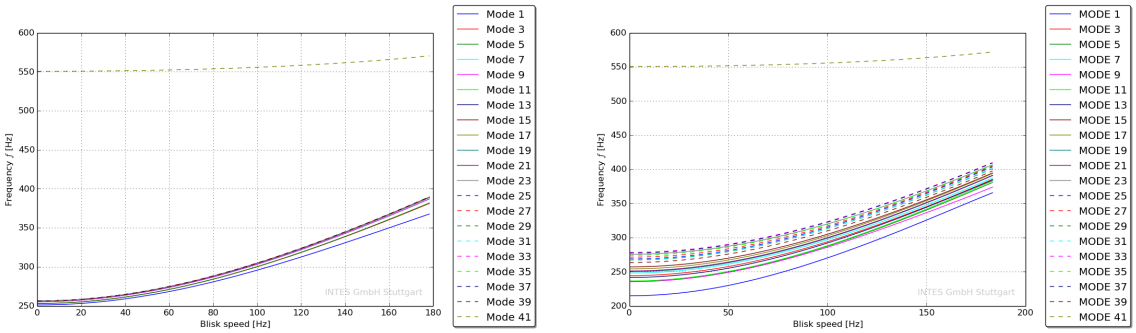

(a) *Tuned blisk* (b) Mistuned blisk

Figure 7: Campbell diagrams

All variables are assumed to be independent and normally distributed. The limit state function

$$g(\boldsymbol{X}) = w_{\text{max}} - w(\boldsymbol{X}) \tag{8}$$

is defined as the difference between the maximum normal tip displacement amplitude at two adjacent blades and a threshold value w_{max} measured in millimeters. By convention the failure domain is defined as the set $\{F\} = \{g(\boldsymbol{X}) \leq 0\}$. The limit state surface $g(\boldsymbol{X}) = 0$ separates failure and survival domain. Fig. (9) illustrates the limit state surface. Each dot denotes a sampling point. The probability of failure P_F may be defined by the following

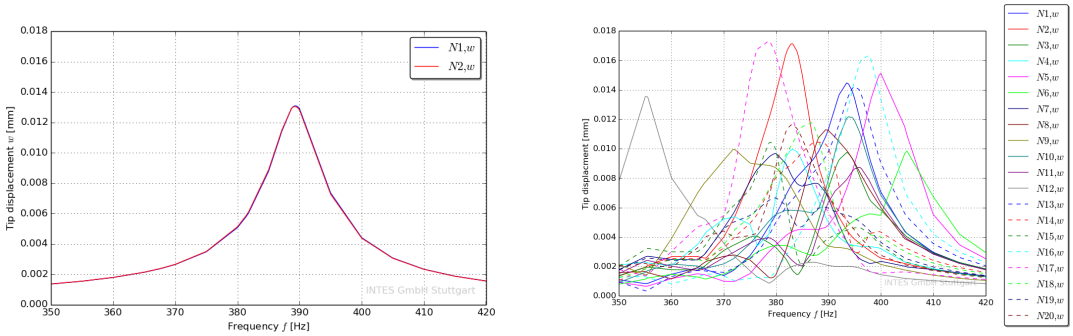

(a) *Tuned blisk* (b) Fully mistuned blisk

Figure 8: Forced response of an ideal bisk and a fully mistuned blisk with 20 basic variables ($\Omega = 10700$ rpm)

Table 2: Statistical properties of random variables

Variable	Type of distribution	Units	Mean value μ	Standard deviation σ
X_1	Normal	[Pa]	$1.1024\,10^{11}$	$1.1024\,10^{10}$
X_2	Normal	[Pa]	$1.1024\,10^{11}$	$1.1024\,10^{10}$

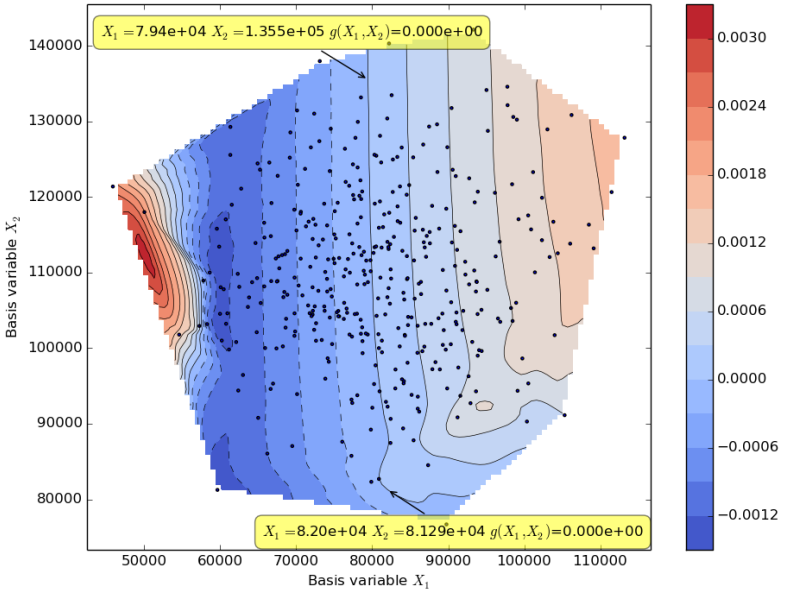

Figure 9: Limit state surface obtained by an adaptive Monte Carlo simulation

integral:

$$P_F = \int\limits_{g(\boldsymbol{X})\leq 0} f_{\boldsymbol{X}}(\boldsymbol{x})\mathrm{d}\boldsymbol{x}, \tag{9}$$

where $f_{\boldsymbol{X}}(\boldsymbol{x})$ is the joint probability density function of the random variables $\boldsymbol{X}$. The integral in (9) is usually rewritten by means of an indicator function

$$I[g(\boldsymbol{X})] = \begin{cases} 1 & g(\boldsymbol{X}) \leq 0 \\ 0 & g(\boldsymbol{X}) > 0 \end{cases}, \tag{10}$$

where the integration domain is changed to the entire sample space of $\boldsymbol{X}$:

$$P_F = \int I[g(\boldsymbol{X})]\, f_{\boldsymbol{X}}(\boldsymbol{x}) \mathrm{d}\boldsymbol{x}. \tag{11}$$

Thus an estimator of the failure probability is given by

$$\widetilde{P}_F = \frac{1}{N} \sum_{j=1}^{N} I[g(\boldsymbol{X}) \leq 0]. \tag{12}$$

By the strong law of large numbers, this sample mean converges almost surely to the integral (11) as N approaches to infinity. During simulation, after each sample the reliability data are written on ASCII files. The reliability analysis for one failure function is stopped if reliability is determined with the desired covariance of simulation Fig (10). The relation between the probability of failure P_F and the reliability index β is given by

$$P_F = \Phi(-\beta) = 1 - \Phi(\beta), \tag{13}$$

where $\Phi(.)$ is the cumulative distribution function of the standard normal variate. The coefficient of variation (CV) is defined as the ratio of the standard deviation σ to the mean μ.

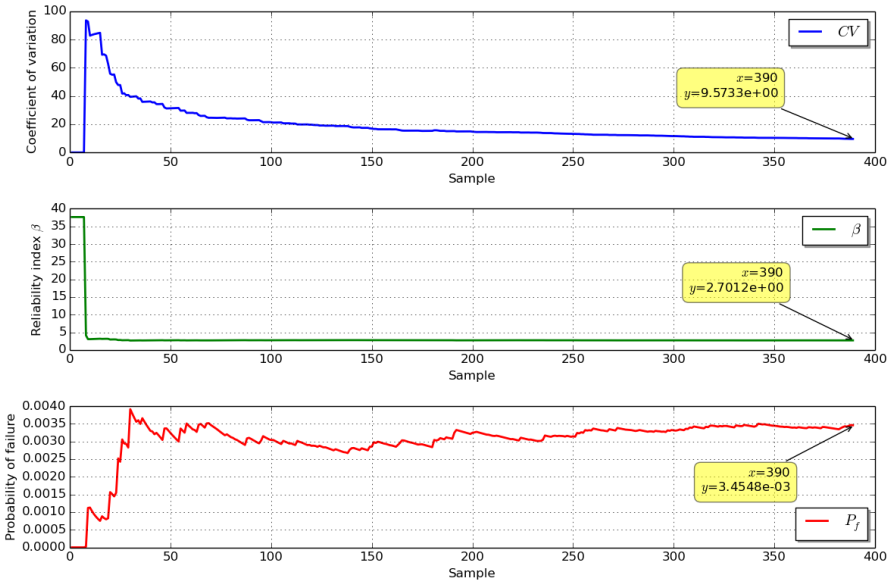

Figure 10: Intermediate results of an adaptive Monte Carlo simulation

5 Conclusion

The mistuning effect on the free and forced response is studied by a reliability approach. The failure probability for a mistuned blisk is computed by an adaptive Monte Carlo method. All the necessary tools are provided by PERMAS/VisPER to perform reliability analyses in a seamless process chain.

REFERENCES

[1] Abdul-Aziz, A. Trudell J. J., Baakilini, G. Y. (2005) Finite element design study of a bladed, flat rotating disk to simulate cracking in a typical turbine disk. *Proc. SPIE, Nondestructive Evaluation and Health Monitoring of Aerospace Materials, Composites, and Civil Infrastructure IV*, Vol. 5767

[2] Bhartiya, Y., Sinha, A. (2014) Accuracies of reduced order models of a bladed rotor with geometric mistuning. *Journal of Turbomachinery*, **136**

[3] Castanier, M. P., Pierre, C. (2006) Modeling and analysis of mistuned bladed disk vibration: Status and emerging directions. *Journal of Propulsion and Power*, **22**, pp. 384–396

[4] Gollwitzer, S., Kirchgäßner, B., Fischer, R., Rackwitz, R. (2006) PERMAS-RA/STRUREL system of programs for probabilistic reliability analysis. *Structural Safety*, **28**, pp. 108–129.

[5] Ganine, V., Legrand, M., Michalska, H., Pierre, C. (2009): A sparse preconditioned iterative method for vibration analysis of geometrically mistuned bladed disks, *Computers and Structures*, **87**, pp. 342–354.

[6] Huang, S. C., Chiu, Y.-J. (2007): Shaft-torsion and blade-beding coupling vibrations in a rotor system with grouped blades. *Journal of System Design and Dynamicd*, **1**, pp. 748–759

[7] Ismail, A. E., Ariffin, A. K., Abdullah, S., Ghazali, M. J. (2011): Probabilistic assessments of the plate using Monte Carlo simulation. *Materials Science and Engineering*, **17**.

[8] Karatas, H. C., Cigeroglu, E., Özgüven, H. N. (2012): Possibilistic interpretation of mistuning in bladed disks by fuzzy algebra. *Proc. IMAC XXX* Jacksonville Florida, USA, Jan. 30 - Feb. 2

[9] Khemiri, O., Martel, C., Corral, R. (2013): Asymptotic description of damping mistuning effects on the forced response of turbomachinery bladed discs. *Journal of Sound and Vibration*, **332**, pp. 4998–5013

[10] Laxalde, D., Lombard, J.-P., Thouverez, F. (2007): Dynamics of multistage bladed disk systems. *Journal of Engineering for Gas Turbines and Power*, **129**, pp. 1058–1064

[11] Laxalde, D., Pierre, C. (2010): Modelling and analysis of multi-stage systems of mistuned bladed disks. *Computers and Structures*, **89**, pp. 316—324

[12] Li, J., Castanier, M. P., Pierre, C., Ceccio, S.L. (2006) Experimental Monte Carlo mistuning assessment of bladed disk vibration using forcing variations. In *47th AIAA/ASME/ASCE/AHS/ASC Structures, Structural Dynamics, and Material Conference*. 1-4 May, Newport, Rhode island.

[13] Lim, S-H., Pierre, C., Castanier, M. P. (2006) Predicting blade stress levels directly from reduced-order vibration models of mistuned bladed disks. *Journal of Turbomachinery*, **128**, pp. 206–210

[14] Lim, S-H., Pierre, C., Castanier, M. P. (2007) Compact, generalized component mode mistuning representation for modeling bladed disk vibration. *AIAA Journal*, **45**, pp. 2285–2298

[15] Madden, A. C., Castanier, M. P., Epureanu, B. I. (2011): Mistuning idenfication of blisks at higher frequencies. *AIAA Journal*, **49**, pp. 1299–1302

[16] McGee III, O. G., Fang, C., El-Aini, Y. (2013) A reduced-order meshless energy model for the vibrations of mistuned bladed disks – Part I: Theoretical Basis. **135**

[17] McGee III, O. G., Fang, C., El-Aini, Y. (2013) A reduced-order meshless energy model for the vibrations of mistuned bladed disks – Part II: Finite element benchmark comparisons. **135**
Journal of Turbomachinery

[18] Mignolet, M. P., Hu, W., Jadic, I. (2000): On the forced response of harmonically and partially mistuned bladed disks. Part I: Harmonic mistuning. *International Journal of Rotating Machinery*, **6**, pp. 29–41

[19] Nikolic, M., Petrov, E. P., Ewins, D. J. (2007): Coriolis forces in forced response analysis of mistuned bladed disks. *Journal of Turbomachinery*, **129**, pp. 730–739

[20] Olson B. J., Shaw, S. W., Shi, C., Pierre, C., Parker, R. G. (2014) Circulant matrices and their application to vibration analysis, *Applied Mechanics Reviews*, **66**

[21] Petrov, E. P., Sanliturk, K. Y., Ewins, D. J. (2002): A new method for dynamic analysis of mistuned bladed disks based on the exact relationship bewteen tuned and mistuned systems. *Journal of Engineering for Gas Turbines and Power*, **124**, pp. 586–597

[22] Petrov, E. P., Ewins, D. J. (2003): Analysis of the worst mistuning patterns in bladed disk assemblies. *Journal of Turbomachinery*, **125**, pp. 623–631

[23] Petrov, E. P. (2008): Explicit finite element models of friction dampers in forced response analysis of bladed discs. *Journal of Engineering for Gas Turbines and Power*, **130**

[24] Petrov, E. P. (2010): A method for forced response analysis of mistuned bladed disks with aerodynamic effects included. *Journal of Engineering for Gas Turbines and Power*, **132**

[25] Petrov, E. P. (2011): Reduction of forced response levels for bladed disks by mistuning: overview of the phenomenon. *Journal of Engineering for Gas Turbines and Power*, **133**

[26] Rahimi, M., Ziaei-Rad, S. (2010): Uncertainty treatment in forced response calculation of mistuned bladed disk. *Mathematics and Computers in Simulation* **80**, pp. 1746–1757

[27] Rotea, M. A., DÁmato, F. J. (2003): Efficient algorithms for mistuning analysis. In *Proceedings of the 15th Triennial World Congress*. Barcelona, Spain.

[28] Segui, B., Faverjon, B., Jacquet-Richardet, G. (2013): Effects of random stiffness variations in multistage rotors using the polynomial chaos expansion. *Journal of Sound and Vibration*. **332**, pp. 4178–4192

[29] Shapiro, B. (1999): Solving for mistuned forced response by symmetry. *Journal of Propulsion and Power*, **15**, pp. 310–325

[30] Sinha, A. (2006); Computation of the statistics of forced response of a mistuned bladed disk assembly via polynomial chaos. *Journal of Vibration and Acoustics*, **128**, pp. 449–457.

[31] Sinha, A. (2009): Reduced-order model of a bladed rotor with geometric mistuning. *Journal of Turbomachinery*, **131**

[32] Sinha, A. (2010): Computation of eigenvalues and eigenvectors of a mistuned bladed disk via unidirectional Taylor series expansion. *Journal of Turbomachinery*, **132**

[33] Sternschüss, A., Balmes, E., Jean, P., Lombard, J.-P. (2009): Reduction of multistage disk models: Application to an industrial rotor. *Journal of Engineering for Gas Turbines and Power*, **131**

[34] `http://www.intes.de`